

W boson polarization in vector boson scattering at the LHC

Alessandro Ballestrero,^a Ezio Maina^{a,b} and Giovanni Pelliccioli^{a,b}

^a*INFN, Sezione di Torino,*

Via Giuria 1, 10125 Torino, Italy

^b*Dipartimento di Fisica, Università di Torino,*

Via Giuria 1, 10125 Torino, Italy

E-mail: ballestrero@to.infn.it, maina@to.infn.it, gpellicc@to.infn.it

ABSTRACT: Measuring the scattering of longitudinally-polarized vector bosons represents a fundamental test of ElectroWeak Symmetry Breaking.

In addition to the challenges provided by low rates and large backgrounds, there are conceptual issues which need to be clarified for the definition of a suitable signal. Since vector bosons are unstable and can only be observed through their decay products, the polarization states interfere among themselves. Moreover, already at tree level, there are diagrams which cannot be interpreted as production times decay of EW bosons but are necessary for gauge invariance.

We discuss a possible way to define a cross section for polarized W 's, dropping all non resonant diagrams, and projecting on shell the resonant ones, thus preserving gauge invariance. In most cases, the sum of polarized distributions reproduces the full results. In the absence of cuts, the ratios of the polarized cross sections to the full one agree with the results of a standard projection on Legendre polynomials. While the latter cannot be employed in a realistic environment, a comparison of the data with the shapes of the angular distributions for polarized vector bosons allows the extraction of the polarization fractions in the presence of selection cuts on the charged leptons.

Contents

1	Introduction	1
2	W boson polarization and angular distribution of its decay products	4
3	Separating the resonant contribution: On Shell Projection	6
4	Setup of the simulations	9
5	Validating the approximation in the absence of cuts on the charged leptons	9
6	Joint polarization fractions for the two W's	12
7	Leptonic cuts and their effects	13
8	Determining the polarization fractions	16
9	Conclusions	22
Appendix A Numerical effects of different approximations in the large mass, large transverse momentum region.		22
A.1	Resonant contributions and gauge cancellations	22
A.2	Vector boson widths in the OSP method	27

1 Introduction

The discovery of a scalar particle [1, 2], whose properties are compatible with those of the Higgs Boson [3, 4], represents an historic confirmation of the Standard Model description of ElectroWeak Symmetry Breaking (EWSB). In the SM, vector bosons acquire mass through their coupling to the Higgs field. At the same time, the Higgs is essential in the scattering of vector bosons (VBS), avoiding the divergence at high energy, in the longitudinally-polarized sector, which would be triggered by their very masses. In the SM, the cross section for VBS processes is very small because of cancellations among different contributions. Processes related to new physics can disturb this delicate balance and lead to potentially large enhancements of the VBS rate, making it the ideal process for searches of deviations from the SM and hints of New Physics [5–24].

The experimental results on VBS obtained in Run 1 at the LHC have very low statistics. In the near future, Run 2 will collect data with much better precision. Still, the effects searched for are expected to be very small, therefore improvements of theoretical predictions and experimental strategies will be required.

Understanding from a theoretical point of view how to separate the polarizations of the W 's in VBS is a necessary prerequisite to any effort to perform the separation in the data. In particular, it would be useful to isolate the longitudinal component where deviations from the SM are larger and easier to reveal.

The basic tool has been known for a long time: each of the three on shell polarizations results in a specific decay distribution of the charged leptons. Two obstructions, however, hamper progress along this path:

- Since the W 's are unstable particles, the decays of the individual polarizations interfere among themselves, even in the limit of narrow width. These interference contributions cancel exactly only when an integration over the full azimuth of the lepton is performed. Acceptance cuts, however, inhibit collecting data over the full angular range. In addition, cuts affect differently the three polarizations and modify the angular distributions. Notice that the effects discussed here are present in every W production channel, not only in VBS.
- With few exceptions, ElectroWeak boson production processes are described by amplitudes including non resonant diagrams, which cannot be interpreted as production times decay of any vector boson, as shown in fig. 1(c) for the VBS case. These diagrams are essential for gauge invariance and cannot be ignored. For them, separating polarizations is simply unfeasible. Furthermore, as it will be shown later, their contribution is, in general, not negligible.

The polarization fractions in the SM for $W + jets$ processes, without cuts on the charged leptons, have been discussed in ref. [25]. The effects of selection cuts have been studied in ref. [26] for $W + jets$ and a number of other W production mechanisms. The analysis in ref. [26] showed how the decay distributions of the charged leptons get distorted by the presence of cuts and how the simple methods that allow to measure the polarization components when no cut on the charged leptons is imposed, fail when cuts are introduced. The interplay between interference among W polarizations and selection cuts has been also examined in ref. [27].

A number of measurements of the polarization fractions of the W have been performed at the LHC, both by CMS [28] and ATLAS [29], in the $W + jets$ channel. Both collaborations have also studied the polarization of the W 's [30, 31] in top-antitop events.

It should be mentioned that the charged lepton decay angles cannot be measured exactly because of the difficulties in reconstructing the center of mass frame of the W . Therefore, in practice, other, directly observable, quantities are studied as proxies. Examples are L_P [28], $\cos \theta_{2D}$ [29] and R_{p_T} [32], which is mostly useful for the W^+W^+ channel.

In this paper, we discuss under which conditions it is possible to define VBS cross sections for polarized W 's, and study their basic properties at the LHC. We also show how to overcome the difficulties related to the presence of acceptance cuts for the charged leptons. We believe these preliminary steps to be essential for this kind of measurement.

We are far from being fully realistic. Nonetheless, our results pave the way to future phenomenological analyses. We limit ourselves to the simple case of W^+W^- production

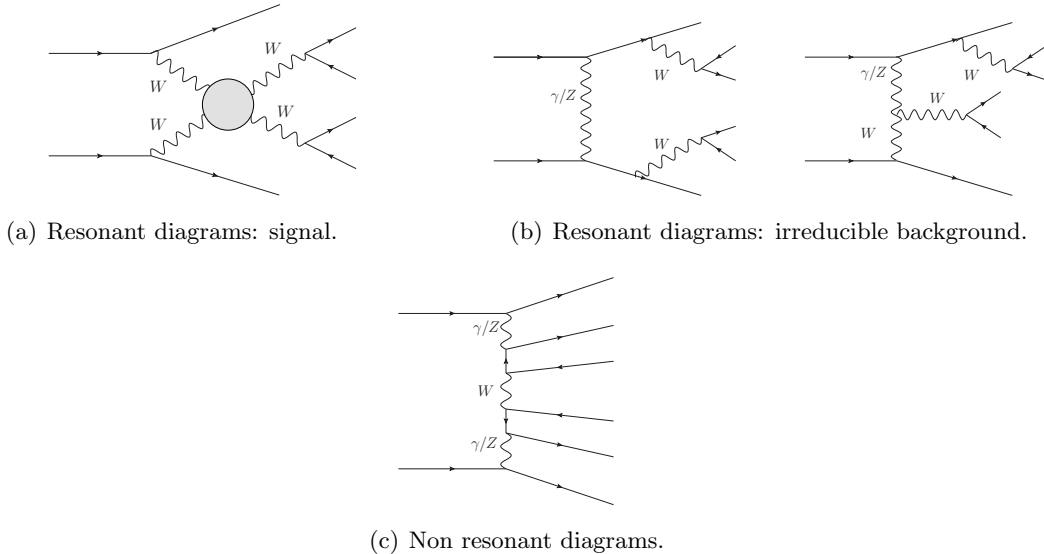


Figure 1. Representative diagrams for WW scattering.

in VBS when both vector bosons decay leptonically. We also consider only the case in which the two leptons are an $e^-\mu^+$ pair, which avoids the small complication of the Z contribution which appears when the two leptons belong to the same family. A cut on the mass of the two leptons would suffice to completely eliminate this channel.

While the leptonic decay of the W 's leads to a cleaner environment, the presence of two neutrinos makes the estimate of the invariant mass of the boson boson system more involved. Some of these difficulties might be alleviated studying the semileptonic channel instead of the fully leptonic one. However, in the semileptonic case the QCD background is larger and it is difficult to separate WW from WZ production. In addition, one of the two vector bosons needs to be identified from its hadronic decay.

The present study could be easily extended to include NLO QCD corrections [33, 34] since they do not modify the W decay. EW corrections, which have been recently calculated [35] for same sign W 's, potentially mix the production and decay part of the amplitudes and will require an additional effort.

We are confident that if separation between the different polarizations can be achieved in Monte Carlo simulations it will also be within reach of the experiments, given sufficient luminosity.

The structure of the paper is the following: in the next section we recall how the polarizations of the W 's enter the amplitudes when the decay is taken into account exactly and how interferences between polarizations arise. Next, we present the approximations which we propose in order to separate the different polarizations and show how they reproduce the full result in the absence of cuts on the leptons. In particular we discuss how the full differential distributions are reproduced, in most cases, by the sum of singly polarized distributions with the exception of those variables, like the charged lepton transverse momentum, which constrain the available angular range for the decay. In sect. 7 we introduce acceptance leptonic cuts and discuss how they spoil the cancellation of the interference

contributions and modify the simple form of the decay angular distribution. Finally, in sect. 8 we show that the shapes of the angular decay distributions are sufficiently universal to allow an almost model independent measurement of the polarization fractions. We extract the polarization components in the Higgsless model and in one instance of a Singlet extension of the SM, fitting the full distribution with a sum of singly polarized SM shapes.

2 W boson polarization and angular distribution of its decay products

As already mentioned, a vector boson production tree level reaction, in general, receives contribution from different classes of diagrams, both resonant and non resonant. If we concentrate on hadronic processes at $\mathcal{O}(\alpha_{EM}^2 \alpha_S^n)$, involving a single intermediate W^+ which decays leptonically, each diagram includes one ElectroWeak propagator of timelike momentum. The amplitude can be written, in the Unitary Gauge, as

$$\mathcal{M} = \mathcal{M}_\mu \frac{i}{k^2 - M^2 + i\Gamma M} \left(-g^{\mu\nu} + \frac{k^\mu k^\nu}{M^2} \right) \left(\frac{-ig}{2\sqrt{2}} \bar{\psi}_l \gamma_\nu (1 - \gamma^5) \psi_{\nu_l} \right), \quad (2.1)$$

where M and Γ are the W mass and width, respectively.

The polarization tensor can be expressed in terms of four polarization vectors [36]

$$-g^{\mu\nu} + \frac{k^\mu k^\nu}{M^2} = \sum_{\lambda=1}^4 \varepsilon_\lambda^\mu(k) \varepsilon_\lambda^{\nu*}(k). \quad (2.2)$$

In a frame in which the off shell W boson propagates along the z -axis, with momentum κ , energy E and invariant mass $\sqrt{Q^2} = \sqrt{E^2 - \kappa^2}$, the polarizations read:

$$\begin{aligned} \varepsilon_L^\mu &= \frac{1}{\sqrt{2}}(0, +1, -i, 0) \text{ (left)}, \\ \varepsilon_R^\mu &= \frac{1}{\sqrt{2}}(0, -1, -i, 0) \text{ (right)}, \\ \varepsilon_0^\mu &= (\kappa, 0, 0, E)/\sqrt{Q^2} \text{ (longitudinal)}, \\ \varepsilon_A^\mu &= \sqrt{\frac{Q^2 - M^2}{Q^2 M^2}}(E, 0, 0, \kappa) \text{ (auxiliary)}. \end{aligned} \quad (2.3)$$

The longitudinal and transverse polarizations obey the standard constraints $\varepsilon_i \cdot k = 0$, $\varepsilon_i \cdot \varepsilon_j^* = -\delta_{i,j}$, $i, j = 0, L, R$. The auxiliary polarization ε_A^μ satisfies $\varepsilon_A \cdot \varepsilon_i^* = 0$, $i = 0, L, R$, $\varepsilon_A \cdot \varepsilon_A^* = (Q^2 - M^2)/M^2$, $\varepsilon_A \cdot k = \sqrt{(Q^2 - M^2) Q^2}/M^2$.

On shell, the auxiliary polarization is zero and the longitudinal polarization reduces to the usual expression: $\varepsilon_0^\mu = (\kappa, 0, 0, E)/M_W$. The most general case, in which the W propagates along a generic direction, can easily be obtained by a rotation.

The decay amplitudes of the W ,

$$\mathcal{M}^\mathcal{D}_\lambda = \frac{-ig}{2\sqrt{2}} \bar{\psi}_l \varepsilon_\lambda^{\mu*} \gamma_\mu (1 - \gamma^5) \psi_{\nu_l}, \quad (2.4)$$

depend on its polarization. In the rest frame of the $\ell\nu$ pair, they are:

$$\mathcal{M}^{\mathcal{D}}_0 = ig \sqrt{2} E \sin \theta , \quad (2.5)$$

$$\mathcal{M}^{\mathcal{D}}_{R/L} = ig E (1 \pm \cos \theta) e^{\pm i\phi} , \quad (2.6)$$

where (θ, ϕ) are the charged lepton polar and azimuthal angles, respectively, relative to the boson direction in the laboratory frame. The decay amplitude for the auxiliary polarization is zero, for massless leptons, because ε_A^μ is proportional to the four-momentum of the virtual boson. Hence, each physical polarization is uniquely associated with a specific angular distribution of the charged lepton, even when the W boson is off mass shell.

Defining a polarized production amplitude,

$$\mathcal{M}^{\mathcal{P}}_\lambda = \mathcal{M}_\mu \varepsilon_\lambda^\mu , \quad (2.7)$$

the full amplitude can be written as:

$$\mathcal{M} = \sum_{\lambda=1}^3 \mathcal{M}^{\mathcal{P}}_\lambda \frac{i}{k^2 - M^2 + i\Gamma_w M} \mathcal{M}^{\mathcal{D}}_\lambda = \sum_{\lambda=1}^3 \mathcal{M}^{\mathcal{F}}_\lambda , \quad (2.8)$$

where $\mathcal{M}^{\mathcal{F}}_\lambda$ is the full amplitude with a single polarization for the intermediate W . Notice that in each $\mathcal{M}^{\mathcal{F}}_\lambda$ all correlations between production and decay are exact.

The squared amplitude becomes:

$$\underbrace{|\mathcal{M}|^2}_{\text{coherent sum}} = \underbrace{\sum_{\lambda} |\mathcal{M}^{\mathcal{F}}_\lambda|^2}_{\text{incoherent sum}} + \underbrace{\sum_{\lambda \neq \lambda'} \mathcal{M}^{\mathcal{F}*}_\lambda \mathcal{M}^{\mathcal{F}}_{\lambda'}}_{\text{interference terms}} . \quad (2.9)$$

The interference terms in eq.(2.9) are not, in general, zero. They cancel only when the squared amplitude is integrated over the full range of the angle ϕ , or, equivalently, when the charged lepton can be observed for any value of ϕ . This remains true in the Narrow Width Approximation in which $1/((k^2 - M^2)^2 + \Gamma_w^2 M^2)$ is replaced by $\pi \delta(k^2 - M^2)/(\Gamma M)$. With this substitution, the integration over the invariant mass of the intermediate state becomes trivial, but the angular integration is unaffected.

If we denote by $d\sigma(\theta, \phi, X)/dLips$ the fully differential cross section, where θ, ϕ are the W decay variables in the boson rest frame and X stands for all additional phase space variables, by $d\sigma(\theta, X)/d\cos\theta/dX$ its integral over ϕ ,

$$\frac{d\sigma(\theta, X)}{d\cos\theta dX} = \int d\phi \frac{d\sigma(\theta, \phi, X)}{dLips} , \quad (2.10)$$

and by $d\sigma(X)/dX$ the integral of $d\sigma(\theta, X)/d\cos\theta/dX$ over $\cos\theta$,

$$\frac{d\sigma(X)}{dX} = \int d\cos\theta \frac{d\sigma(\theta, X)}{d\cos\theta dX} , \quad (2.11)$$

one can write, using eq.(2.5) and eq.(2.6),

$$\frac{1}{\frac{d\sigma(X)}{dX}} \frac{d\sigma(\theta, X)}{d\cos\theta dX} = \frac{3}{8} (1 \mp \cos\theta)^2 f_L(X) + \frac{3}{8} (1 \pm \cos\theta)^2 f_R(X) + \frac{3}{4} \sin^2\theta f_0(X) , \quad (2.12)$$

where the upper sign is for W^+ and the lower sign for W^- . In general the f_i depend on the variables X which are not integrated over. The normalizations are chosen so that

$$\frac{1}{\frac{d\sigma(X)}{dX}} \int_{-1}^1 d\cos\theta \frac{d\sigma(\theta, X)}{d\cos\theta dX} = f_L + f_0 + f_R = 1 \quad (2.13)$$

and f_L , f_0 and f_R represent the left, longitudinal and right polarization fractions, respectively. The steps which lead to eq.(2.12) can be repeated even when a partial or complete integration over the X variables is performed.

If eq.(2.12) holds, the polarized components can be extracted from the differential angular distribution by a projection on the first three Legendre polynomials:

$$\frac{1}{\sigma} \frac{d\sigma}{d\cos\theta} = \sum_{l=0}^2 \alpha_l P_l(\cos\theta), \quad \alpha_l = \frac{2l+1}{2} \int_{-1}^1 d\cos\theta \frac{1}{\sigma} \frac{d\sigma}{d\cos\theta} P_l(\cos\theta). \quad (2.14)$$

This procedure is completely equivalent to the method used in refs. [25, 26] based on the calculation of the first few moments of the angular distribution.

The polarization fractions f_0, f_L, f_R can be obtained as:

$$\begin{aligned} f_0 &= \frac{2}{3}(\alpha_0 - 2\alpha_2), \\ f_L &= \frac{2}{3}(\alpha_0 \mp \alpha_1 + \alpha_2), \\ f_R &= \frac{2}{3}(\alpha_0 \pm \alpha_1 + \alpha_2), \end{aligned} \quad (2.15)$$

where the upper/lower sign refers to the W^+/W^- . We note that the sum $f_0 + f_R + f_L = 2\alpha_0$ is bound to be one.

A word of caution is necessary when acceptance cuts are imposed on the charged leptons, as is unavoidable in practice. While the cancellation of the interference terms in eq.(2.9) is a necessary condition for the validity of eq.(2.12), this is by no means sufficient. A generic cut, think of the lepton transverse momentum, will depend on both the angular variables and the variables X . Integrating over X , in the presence of cuts, results in a different theta dependence. As a consequence, the measured lepton decay distribution is not described any more by the simple formula eq.(2.12) and the polarization fractions cannot be computed as in eq.(2.15).

In order to separate the polarized components in the data, it is necessary to compute the individual amplitudes $\mathcal{M}^{\mathcal{F}}_\lambda$ in eq.(2.8), which requires making the substitution

$$\sum_{\lambda'} \varepsilon_{\lambda'}^\mu \varepsilon_{\lambda'}^{\nu*} \rightarrow \varepsilon_\lambda^\mu \varepsilon_\lambda^{\nu*}. \quad (2.16)$$

in the W propagator. For the present analysis, this possibility has been introduced in PHANTOM [37].

3 Separating the resonant contribution: On Shell Projection

After our discussion of W boson polarization in processes with a single W , we now turn to reactions which contain non resonant diagrams, in particular to those in which two lepton

pairs, $e^- \bar{\nu}_e$ and $\mu^+ \nu_\mu$, are produced. For the set of diagrams in which each leptonic line is connected to a single intermediate W , as in figs. 1(a), 1(b), which we will call doubly resonant or just resonant for short, one can proceed as in the previous section. However, there are many diagrams, like the one shown in fig. 1(c), which cannot be expanded in a similar fashion. The only way to proceed, in order to define amplitudes with definite W polarization, is to devise an approximation to the full result that only involves doubly resonant diagrams.

There are, obviously, several conceivable approximations. The simplest one is simply to drop all non resonant diagrams, possibly restricting the mass of the lepton pair in the decay to lie close to the W mass. Since this procedure clearly violates gauge invariance, one expects it would produce distinctly wrong cross sections, at least in particular regions of phase space. For this reason we have chosen an On Shell Projection (OSP) method, which is more commonly known as the pole scheme or pole approximation in the literature. For instance, it has been employed for the calculation of EW radiative corrections to W^+W^- production in refs.[38–42]. This can be realized as a completely gauge invariant approximation.

The procedure can be summarized as follows:

$$\begin{aligned}
\mathcal{M} &= \mathcal{M}_{\text{res}} + \mathcal{M}_{\text{nonres}} = \\
&= \frac{\sum_{\lambda_1, \lambda_2} \mathcal{M}_{\mu\nu}^{\mathcal{P}}(k_1, k_2, X) \varepsilon_{\lambda_1}^\mu(k_1) \varepsilon_{\lambda_2}^\nu(k_2) \varepsilon_{\lambda_1}^{*\alpha}(k_1) \varepsilon_{\lambda_2}^{*\beta}(k_2) \mathcal{M}_\alpha^{\mathcal{D}}(k_1, X_1) \mathcal{M}_\beta^{\mathcal{D}}(k_2, X_2)}{(k_1^2 - M_W^2 + i\Gamma_W M_W)(k_2^2 - M_W^2 + i\Gamma_W M_W)} + \mathcal{M}_{\text{nonres}} \\
&\rightarrow \frac{\sum_{\lambda_1, \lambda_2} \mathcal{M}_{\mu\nu}^{\mathcal{P}}(\bar{k}_1, \bar{k}_2, X) \varepsilon_{\lambda_1}^\mu(\bar{k}_1) \varepsilon_{\lambda_2}^\nu(\bar{k}_2) \varepsilon_{\lambda_1}^{*\alpha}(\bar{k}_1) \varepsilon_{\lambda_2}^{*\beta}(\bar{k}_2) \mathcal{M}_\alpha^{\mathcal{D}}(\bar{k}_1, \bar{X}_1) \mathcal{M}_\beta^{\mathcal{D}}(\bar{k}_2, \bar{X}_2)}{(k_1^2 - M_W^2 + i\Gamma_W M_W)(k_2^2 - M_W^2 + i\Gamma_W M_W)} \\
&= \frac{\sum_{\lambda_1, \lambda_2} \mathcal{M}_{\lambda_1, \lambda_2}^{\mathcal{P}}(\bar{k}_1, \bar{k}_2, X) \mathcal{M}_{\lambda_1}^{\mathcal{D}}(\bar{k}_1, \bar{X}_1) \mathcal{M}_{\lambda_2}^{\mathcal{D}}(\bar{k}_2, \bar{X}_2)}{(k_1^2 - M_W^2 + i\Gamma_W M_W)(k_2^2 - M_W^2 + i\Gamma_W M_W)} = \mathcal{M}_{\text{OSP}}, \tag{3.1}
\end{aligned}$$

where \bar{k}_i is the on mass shell projection of k_i . Here X_i , $i = 1, 2$ stand for the lepton momenta, while X refer to the initial and final quark momenta. \bar{X}_i refer to the lepton momenta after the projection, when the momentum of each $\ell\nu$ pair in the calculation of \mathcal{M}_{res} is on the W mass shell momentum. $\mathcal{M}_{\text{nonres}}$, which includes all singly resonant and non resonant diagrams, is dropped. The denominator in each W propagator is left untouched.

The projected production and decay amplitudes,

$$\mathcal{M}_{\lambda_1, \lambda_2}^{\mathcal{P}}(\bar{k}_1, \bar{k}_2, X) = \mathcal{M}_{\mu\nu}^{\mathcal{P}}(\bar{k}_1, \bar{k}_2, X) \varepsilon_{\lambda_1}^\mu(\bar{k}_1) \varepsilon_{\lambda_2}^\nu(\bar{k}_2), \tag{3.2}$$

$$\mathcal{M}_{\lambda_1}^{\mathcal{D}}(\bar{k}_1, \bar{X}_1) = \varepsilon_{\lambda_1}^{*\alpha}(\bar{k}_1) \mathcal{M}_\alpha^{\mathcal{D}}(\bar{k}_1, \bar{X}_1) \tag{3.3}$$

are ordinary, complete amplitudes with polarized, on shell, external W bosons. Therefore, the final expression is gauge invariant provided $\mathcal{M}^{\mathcal{P}}$ and $\mathcal{M}^{\mathcal{D}}$ are both invariant.

However, this projection is not uniquely defined. As the momentum of a vector boson is sent to mass shell at least the momenta of its two decay products need to be adjusted. One can keep fixed the direction of particle one or of particle two in the overall center of mass. Alternatively one can keep fixed the angles in the center of mass of the vector boson.

These three procedures lead to different momenta of the decay products and therefore to different matrix elements.

In order to have an unambiguous prescription we have chosen to conserve:

1. the total four-momentum of the WW system (thus, also M_{WW} is conserved);
2. the direction of the two W bosons in the WW center of mass frame;
3. the angles of each charged lepton, in the corresponding W center of mass frame, relative to the boson direction in the lab.

Since the original W momenta are typically only slightly off shell, the modification of the kinematics is expected, in most cases, to be minimal. The modified momenta affect only the calculation of the weight of the event. In the LHA event file [43] all particles are assigned the original, unprojected momenta. This procedure can only be applied for $M_{2\ell 2\nu} > 2M_W$. In the following we will refer to the total invariant mass of the four leptons as M_{WW} , for simplicity.

The OSP requires a further adjustment in the computation of the projected amplitudes. In the full calculation, the presence of unstable, intermediate, timelike W and Z bosons, forces the introduction of an imaginary part, typically $-i\Gamma M$ in tree level processes, into their propagators. This corresponds to the partial resummation of a particular class of higher order contributions, effectively mixing different perturbative orders, and has the collateral effect of complicating the issue of gauge invariance [44–46].

When massive vector bosons appear only as virtual states, a simple and effective way of preserving gauge invariance is the Complex Mass Scheme (CMSc) [40, 47]. In the CMSc, all occurrences of the vector boson mass M are replaced by $\sqrt{M^2 - i\Gamma M}$. This includes the cosine of the Weinberg mixing angle and all quantities which are defined in terms of $\cos\theta_W$.

The CMSc, however, is not gauge invariant for amplitudes with external Weak gauge bosons, which are implicitly regarded as stable. The simplest process which exemplifies these issues is $e^+\nu_e \rightarrow W^+\gamma$. If the polarization vector of the photon is substituted by its momentum, the amplitude should become zero, because of the electromagnetic Ward identity. It is easily verified that this happens only if $\Gamma_W = 0$. In the end, gauge invariance forces all widths of intermediate vector bosons in the OSP amplitudes to be set to zero. As a consequence all weak bosons whose momentum can get on their mass shell must be projected on shell simultaneously.

In Appendix A we discuss, in a more quantitative and detailed way, the pitfalls of the non fully gauge invariant approximations mentioned in this section. In the Appendix we focus on the high transverse momentum, high mass region where gauge violating effects are expected to be magnified, particularly when longitudinally polarized vector bosons are involved.

All results, in the following, which are labeled as full have been obtained in the CMSc. All OSP results have been obtained projecting on mass shell all resonant vector bosons, setting to zero all widths in non resonant propagators and using real couplings.

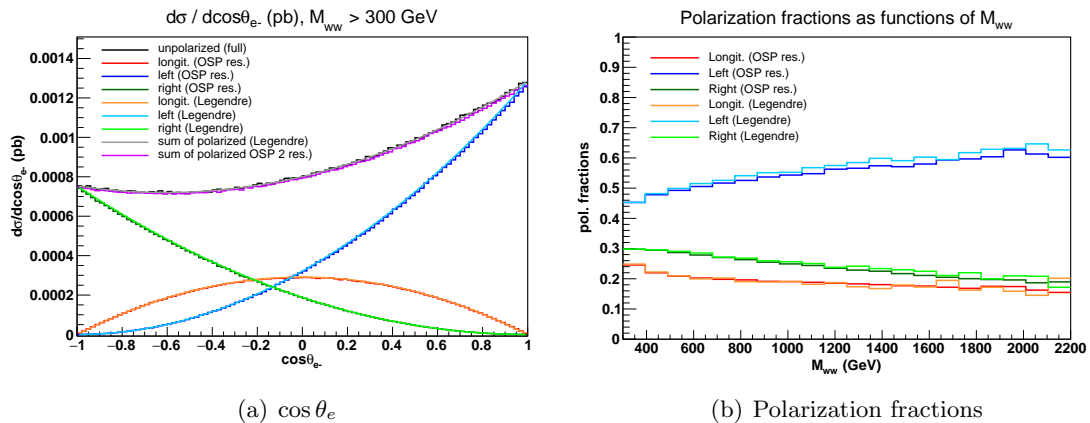


Figure 2. Distribution of electron $\cos\theta$ in the W^- reference frame (left), polarization fractions as functions of M_{WW} (right). The polarization components obtained by expanding the full angular distribution on Legendre polynomials are shown in lighter colors. The darker histograms are obtained integrating the polarized amplitudes squared. The positively charged W is unpolarized.

4 Setup of the simulations

We have studied $pp \rightarrow jj e^- \bar{\nu}_e \mu^+ \nu_\mu$ at parton level. All events have been generated with PHANTOM [37], using the NNPDF30_lo_as_0130 PDF set [48] with scale $Q = M_{WW}/\sqrt{2}$. We consider only ElectroWeak processes at $\mathcal{O}(\alpha_{EM}^6)$. We neglect $\mathcal{O}(\alpha_{EM}^4 \alpha_S^2)$ processes and exclude the top–antitop background assuming perfect b quark veto.

All results shown in this paper refer to the LHC@13TeV and have been obtained with the following set of standard cuts for the hadronic part:

- maximum jet pseudorapidity, $|\eta_j| < 5$;
- minimum jet transverse momentum, $p_t^j > 20$ GeV;
- minimum jet–jet invariant mass, $M_{jj} > 600$ GeV;
- minimum jet–jet pseudorapidity separation, $|\Delta\eta_{jj}| > 3.6$;
- opposite sign jet pseudorapidities, $\eta_{j_1} \cdot \eta_{j_2} < 0$.

The OSP requires the mass of the four lepton system to be larger than twice the mass of the W , thus, only events with $M_{WW} > 300$ GeV have been retained. Since we are mainly interested in VBS at large invariant masses, this is not a limitation.

5 Validating the approximation in the absence of cuts on the charged leptons

In this section we compare the differential distributions of a number of kinematic variables obtained from the full matrix element with the incoherent sum of three OSP distributions in which the negatively charged intermediate W boson is polarized while the positively

charged one remains unpolarized. Only doubly resonant diagrams are included for polarized processes. No lepton cut is applied and, as a consequence, the cross section from the incoherent sum of polarized cross sections coincides with the cross section obtained from the coherent sum.

Our aim is:

- to demonstrate that the W polarization fractions obtained with the OSP are in agreement with those obtained from a standard expansion in Legendre polynomials.
- to show that the OSP reproduces well the full cross section and distributions.
- to explore the differences between the individual polarized distributions as a tool to separate them in the data.

The full cross section is 1.748(1) fb while the incoherent sum of singly polarized cross sections is 1.731(1) fb, which differs from the full result by about 1%.

In figs. 2, 3 the black curves refers to the full differential cross sections and the violet ones to the sum of polarized distributions. The individual distributions are shown in red (longitudinal), blue (left) and green (right). We have also computed the coherent sum of the three polarized contributions, which is, in all cases, almost indistinguishable from the full result and, therefore, is not shown.

In fig. 2, on the left, we show the distribution of the decay angle of the electron in the reference frame of the $e^-\nu_e$ pair integrated over the full range $M_{WW} > 300$ GeV. On the right we present the polarization fractions as a function of the invariant mass of the four leptons, which provides additional information since the distributions in fig. 2(a) are dominated by events with relatively small M_{WW} .

The polarization components obtained by expanding the full angular distribution on Legendre polynomials, as discussed in sect. 2, are shown as lighter shade smooth lines in fig. 2(a) and show that the distributions from the polarized generations, in the absence of cuts on the charged leptons, have the expected functional form, and that the polarization fractions extracted from the full results are in excellent agreement with those obtained from the polarized distributions.

Fig. 2(b) presents the polarization fractions of the W^- as a function of M_{WW} . The darker lines show the ratio of the individual polarized cross sections to the full result in each M_{WW} bin; the lighter lines are obtained from a bin by bin expansion on Legendre polynomials of the full result. The two methods agree over the full range. This confirms that the OSP provides reliable results and opens the way to test it in the presence of cuts, where the Legendre expansion is known to fail.

Fig. 2(b) shows that, in the SM, W^- 's produced in VBS are mainly left handed. The fraction of left polarized W^- 's increases with increasing M_{WW} . The fraction of longitudinal and right handed W 's are roughly the same at large invariant masses. The longitudinal fraction is almost constant at about 20%. The right handed component decreases slightly from approximately 30% at $M_{WW} = 400$ GeV to just above 20% at $M_{WW} = 2000$ GeV.

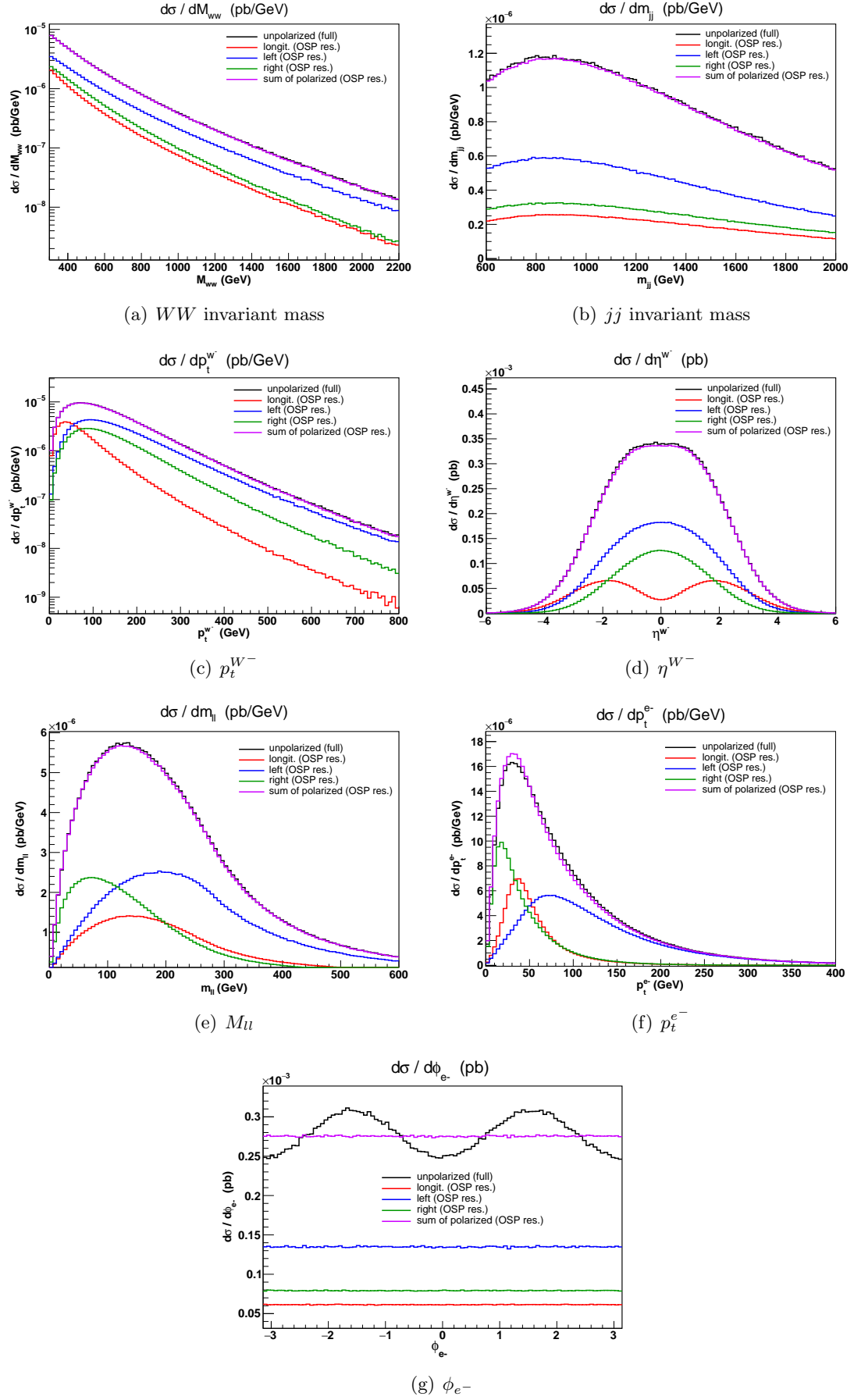


Figure 3. Differential cross sections for $pp \rightarrow jj e^- \bar{\nu}_e \mu^+ \nu_\mu$ at the LHC@13 TeV. Comparison between unpolarized generations based on the full amplitude and the incoherent sum of the polarized generations with OSP, which take into account only the resonant diagrams. No cut on leptonic variables.

The colors in fig. 3 are as in fig. 2: black refers to the full result, violet to the incoherent sum of polarized distributions, red to the longitudinal polarization, blue and green to the left and right polarization, respectively.

The incoherent sum of three OSP distributions agrees very well with the full result for the WW invariant mass, fig. 3(a), the mass of the two tag jets, fig. 3(b), the transverse momentum of the $e^- \nu_e$ pair, fig. 3(c), the rapidity of the $e^- \nu_e$ pair, fig. 3(d) and the mass of the $e\mu$ pair, fig. 3(e).

The agreement is less satisfactory for the transverse momentum of the electron, fig. 3(f). Since, as already mentioned, the coherent sum of the three contributions agrees with the full result, the discrepancy between the black and the violet lines in fig. 3(f) is due to the interference among the different polarizations. The interference is non zero because forcing the lepton p_t to a single bin restricts the angular range of the leptons, spoiling the complete cancellation of the interferences among polarizations.

The distribution, shown in fig. 3(g), of the azimuthal angle of the electron, ϕ_e , which is defined following ref. [25], stands apart. Each of the three singly polarized contributions is isotropic, since the azimuthal angle enters the decay amplitudes only as a phase. The coherent combination of the three amplitudes produces a non trivial modulation of the differential cross section. The incoherent sum of the polarized results reproduces well only the average value of the full distribution.

The singly polarized distributions of the transverse momentum of the W , of its pseudo-rapidity, of the transverse momentum of the negatively charged lepton and of the invariant mass of the two charged leptons depend significantly on the polarization of the W .

Fig. 3(c) shows that longitudinally polarized W 's have a markedly softer p_t spectrum in comparison with transversely polarized ones. In fact they dominate for $p_t^W < 50$ GeV. Fig. 3(d) shows that, while transversely polarized W 's are predominantly produced at small rapidities, the distribution for longitudinally polarized one presents a dip at zero and peaks at $\eta^{W^-} = \pm 2$.

The $p_t^{e^-}$ and M_{ll} distributions are harder for left polarized W^- 's than for longitudinal polarized ones. The right handed W^- 's have the softest spectrum. This behaviour is clearly related to the distribution of decay angles for the three polarizations: the negatively charged leptons from left polarized bosons tend to be produced along the direction of flight of the W , while those originating from right polarized W 's tend to emerge in the opposite direction. The leptons from longitudinally polarized W 's fall in between the two other cases.

6 Joint polarization fractions for the two W 's

The projection described in eqs.(2.14–2.15) can be readily generalized to a simultaneous expansion in products of Legendre polynomials of the two variables $\cos \theta_e$ and $\cos \theta_\mu$. Similarly, the substitution in eq.(2.16) can be performed for each of the two final state W 's. The outcome is shown in fig. 4. For ease of presentation, the right and left handed contributions are summed together in the transverse component $W_T = W_R + W_L$.

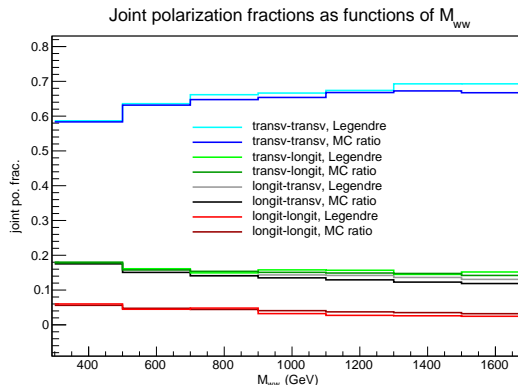


Figure 4. Double polarization fractions as functions of M_{WW} . The right and left handed contributions are summed together in the transverse component $W_T = W_R + W_L$. The polarization components obtained by expanding, in each bin, the full angular distribution on Legendre polynomials are shown in lighter colors. The darker histograms are obtained integrating the polarized amplitudes squared.

The polarization components obtained by expanding, in each bin, the full angular distribution on Legendre polynomials are shown in lighter colors. The darker histograms are obtained integrating the amplitudes squared with definite polarization for each W . The two independent determinations of the joint polarization fractions agree extremely well over the full range in M_{WW} . This implies that the method we propose can be relied on for analyzing double polarized cross sections.

Fig. 4 shows that the $W_T^+ W_T^-$ fraction is always the largest one and dominates at large invariant masses, comprising about 70% of the total cross section. The $W_T^+ W_0^-$ and $W_0^+ W_T^-$ components are essentially equal and almost constant at about 18%. The longitudinal-longitudinal fraction is the smallest one, of the order of a few percent. This implies that measuring the scattering with two longitudinally polarized W 's in the final state, will require determining the polarization of both vector bosons, since a longitudinal W is expected in most cases to be produced in association with a transversely polarized companion.

7 Leptonic cuts and their effects

In this section we document how the distributions presented in sect. 5 are modified by the introduction of realistic acceptance cuts on the electron which is the decay product of the W^- , whose polarization we wish to determine. Our results confirm that the polarization fractions of the W cannot be determined anymore by a projection on the first three Legendre polynomials. We show that, in the presence of standard leptonic cuts, the interference among the polarized amplitudes is small. Therefore, the incoherent sum of the three OSP results approximates fairly well, in most cases, the full distribution.

We require:

$$p_t^e > 20 \text{ GeV}, \quad |\eta^e| < 2.5. \quad (7.1)$$

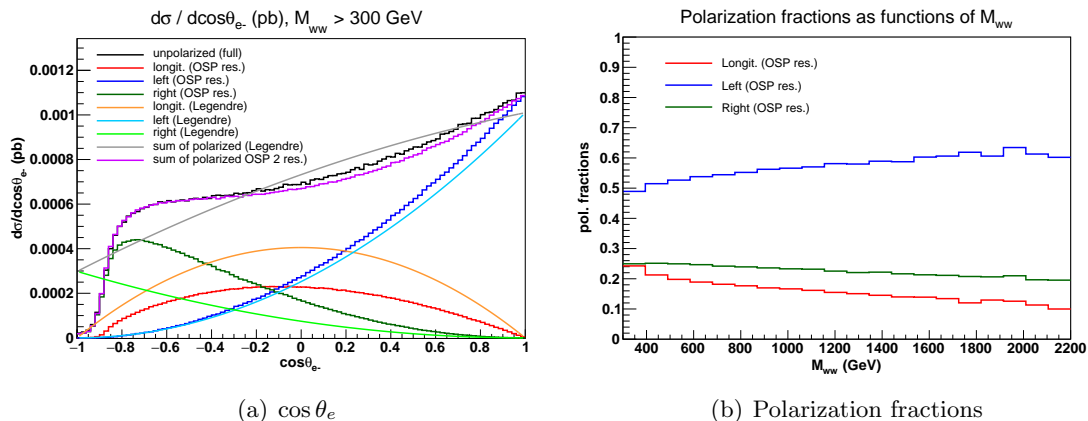


Figure 5. On the left, distributions of $\cos\theta_e$ in the W^- center of mass frame; on the right, the polarization fractions as functions of M_{WW} . $p_t^e > 20$ GeV, $|\eta^e| < 2.5$.

The full cross section is 1.411(1) fb, the coherent sum of OSP polarized amplitudes gives 1.401(1) fb, while the incoherent sum of singly polarized cross sections is 1.382(1) fb, which differs from the full result by about 2%.

In fig. 5 and fig. 6 we show the same set of results presented sect. 5. A number of features are worth noticing. The cross section from the coherent sum of polarized amplitudes is very close to the incoherent sum of cross sections, which indicates that the interference among polarizations is generally small. The rigorous cross section is well reproduced by both approximations.

In fig. 5, on the left, we show the distribution of the decay angle of the electron in the reference frame of the $e^-\nu_e$ pair. On the right we present the polarization fractions as a function of the invariant mass of the four leptons.

The full angular distribution is approximated within a few percent, over the full range, by the sum of the unpolarized results. The full result, shown by the black histogram, however, is not of the form of eq.(2.12) and cannot be described in terms of the three first Legendre polynomials. This becomes clear expanding the full result as in eqs.(2.14–2.15), which yields the blue, green and orange smooth curves in fig. 5. Their sum is the smooth gray curve which fails to describe the correct distribution. As already noticed in ref. [26], when acceptance cuts are imposed, the polarization fractions cannot be reliably extracted from the angular distribution of charged leptons by comparing it to the functional form expected when no cuts are set.

The polarization fractions in fig. 5(b) are computed as the ratio of the individual polarized cross sections to the full result in each M_{WW} bin. An expansion on Legendre polynomials would be meaningless.

The most prominent feature in comparison with the curves on the left hand side of fig. 2 is the depletion at $\cos\theta_e = -1$ in the angular distribution. The right handed component is the one most affected, with the resulting shape substantially different from the $(1 - \cos\theta)^2$ behaviour displayed in the absence of cuts. The bulk of the effect is again related to the preferred direction of emission of the charged leptons from right handed W^- 's, which tend

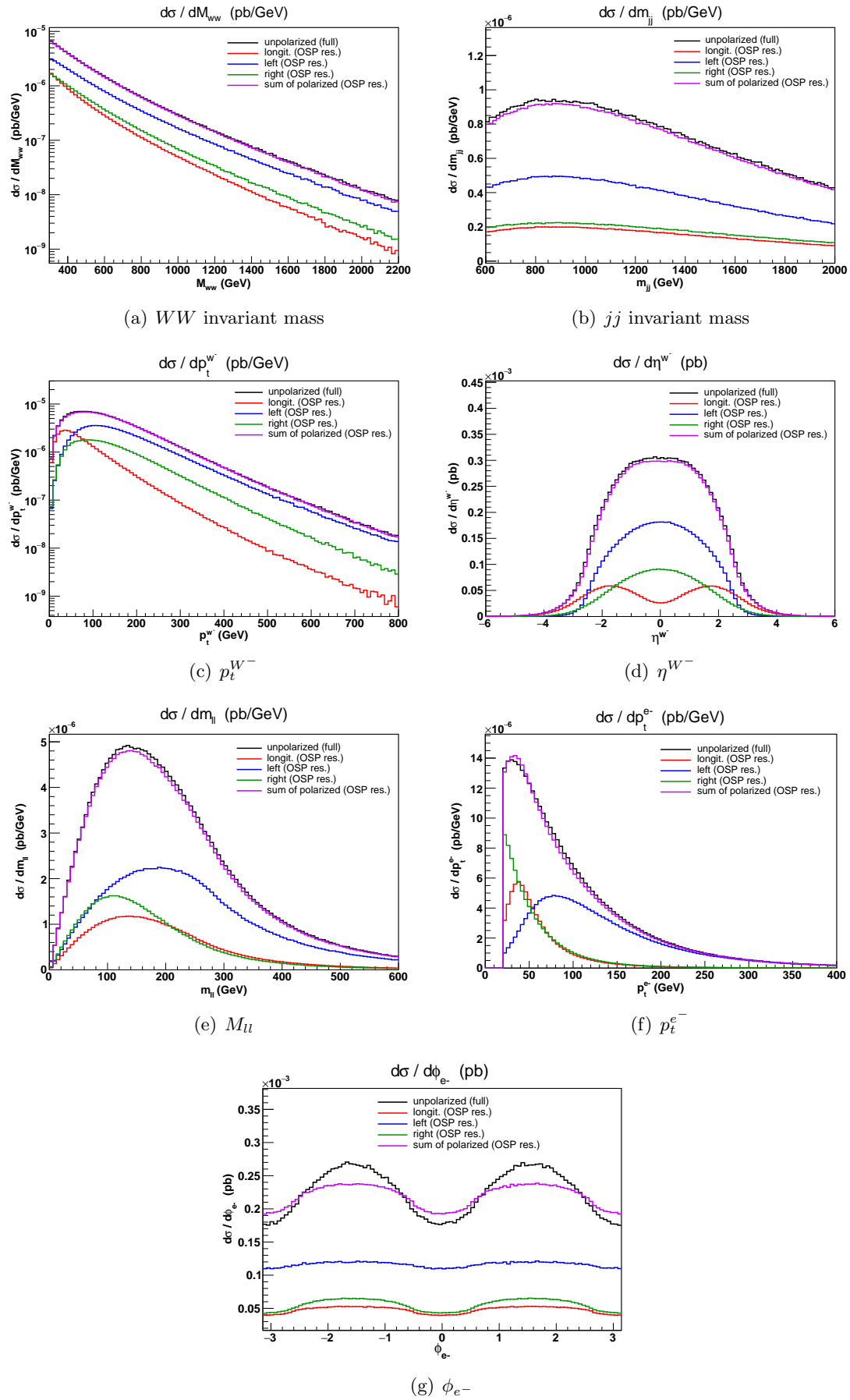


Figure 6. Differential cross sections: comparison between unpolarized and sum of the polarized distributions. $p_t^e > 20$ GeV, $|\eta^e| < 2.5$.

to produce leptons with smaller transverse momentum.

There are, however, subtler effects into play, as can be seen from the polarization fractions as a function of M_{WW} in fig. 5(b). One notices that the longitudinal component decreases faster than the right handed one for increasing M_{WW} . The two curves, which are very close at $M_{WW} < 400$ GeV, separate at large invariant masses, in contrast with the trend they display in fig. 2(b). This is due to the different distribution in W rapidity of the two polarized cross sections. With increasing M_{WW} the average absolute value of the W rapidity with longitudinal polarization increases and a larger number of the corresponding leptons fail the rapidity acceptance cut.

Even in the presence of leptonic cuts, the fraction of longitudinally polarized W^- 's is well above 10%.

The incoherent sum of three OSP distributions agrees well with the full result for the WW invariant mass, fig. 6(a), the mass of the two tag jets, fig. 6(b), the transverse momentum of the $e^- \nu_e$ pair, fig. 6(c), the rapidity of the $e^- \nu_e$ pair, fig. 6(d) and the mass of the $e\mu$ pair, fig. 6(e).

As before, the transverse momentum of the electron, fig. 6(f), is affected by interferences, but the effect is not particularly enhanced by the presence of cuts.

The distribution of the azimuthal angle of the electron in fig. 6(g) displays again peculiar features. Each of the three singly polarized contributions develops a dip at $\phi_e = 0$ and $\phi_e = \pm\pi$. The incoherent combination of the three amplitudes follows more closely the full result than when no cuts are applied but does not reproduce the correct curve.

The individual polarizations are not affected equally by the cuts. Typically, the cross section for right handed W 's is reduced the most, followed by the cross section for longitudinally polarized W 's. Left handed W bosons seem to be the least sensitive to acceptance cuts.

8 Determining the polarization fractions

The fact that the full distribution is well described by the incoherent sum of the polarized differential distributions allows the determination of the polarization fractions within a single model, even in the presence of cuts on the charged leptons. The measured angular distribution can be fitted to a linear combination of the normalized shapes obtained from Monte Carlo simulations of VBS events with final state W 's of definite polarization. We have verified that this procedure works well in the SM for one polarized vector boson. The results shown in sect. 6 suggest that it should be straightforward to extend the method to double polarized events.

However, it would be inconvenient to have to generate templates for all extensions of the SM, being unknown which specific model is realized in nature, should the SM need extending. A natural question is whether this method can provide a model independent, practical way of extracting the polarization fractions from the data, comparable with the Legendre expansion, which is applicable when the W decay is unrestricted by cuts. The essential condition for this approach, is that the shapes of the polarized distributions are sufficiently universal. On one hand, once a polarized W transverse momentum and rapidity

are fixed, its decay is completely specified. Therefore, in any sufficiently small bin in phase space, the angular distribution of the charged lepton will be the same, irrespective of the underlying dynamics. On the other hand, the influence of cuts depends on the transverse momentum and rapidity of the W . Different models yield different distributions of these quantities. Hence, for finite size bins, the details of the averaging over phase space will vary, and some degree of model dependence is to be expected.

In this section we pursue this possibility comparing the distributions produced in the SM with those obtained in different models.

To this purpose, we have studied the Higgsless model obtained from the SM by sending the Higgs mass to infinity. Such model, while not experimentally viable any more, can be viewed as the most extreme modification of the SM in the VBS domain, in which the unitarity violating growth of the scattering of longitudinally polarized vector bosons is completely unmitigated by Higgs exchange.

In figs. 7, 8 we present some results for the Higgsless model. In fig. 7, on the left, we

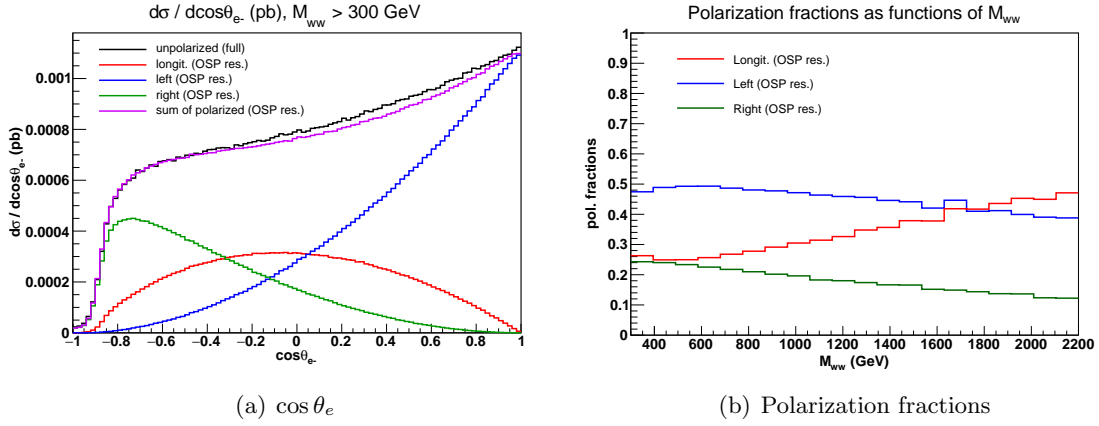


Figure 7. $\cos \theta_e$ distribution (left) and polarization fractions as functions of M_{WW} (right) in the Higgsless model. $p_t^e > 20$ GeV, $|\eta^e| < 2.5$.

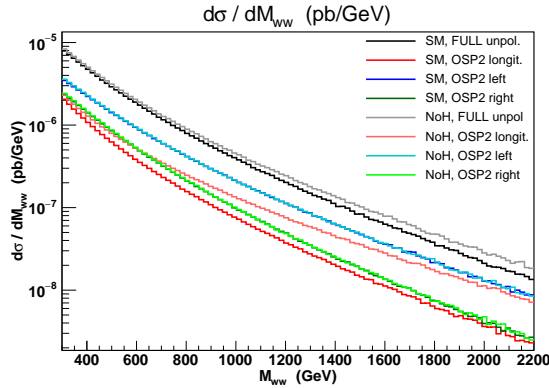


Figure 8. M_{WW} distribution in the Higgsless model compared with the SM results. $p_t^e > 20$ GeV, $|\eta^e| < 2.5$.

show the distribution of the decay angle of the electron in the reference frame of the $e^- \nu_e$ pair. On the right we present the polarization fractions as a function of the invariant mass of the four leptons.

Comparing fig. 7(a) with fig. 5(a), it is immediately evident that the two angular distributions of the charged lepton, in the center of mass of the W , for $M_{WW} > 300$ GeV, are markedly different. The region around $\cos\theta = 0$ is clearly more populated in the Higgsless model as a consequence of a larger fraction of longitudinally polarized bosons. This is confirmed by the comparison between polarization fractions on the right hand side of the two figures. In fig. 7(b) the growth of the longitudinal component is quite prominent. Notice, however, that, even in this extreme model, the left handed fraction is the largest one for all WW invariant masses up to about 1800 GeV.

In fig. 8 we compare the differential cross sections as functions of M_{WW} for the Higgsless model (lighter curves) with the corresponding SM results (darker curves). The full, unpolarized distribution is shown in black/gray. The curves for polarized W^- are given in blue, green and red for the left, right and longitudinal polarization, respectively. The unpolarized cross section for the Higgsless model shows the expected enhancement at large invariant mass with respect to the SM. The comparison of the polarized distributions provides additional information. The differential cross sections for a left or right polarized W^- are identical in the SM and in the Higgsless model. The difference between the full SM result and the Higgsless one is fully accounted for by the difference in the longitudinal component.

The results discussed in the previous sections show that the differential cross section with a definite W^- polarization can be interpreted, up to corrections of a few percent, as the sum of three differential cross sections in which the positively charged W assumes the three possible polarizations. Since the results for a left and right polarized W^- indicate that the absence of the Higgs does not increase the cross section for a transversely polarized W^- and a longitudinally polarized W^+ , the large difference in the cross section for a longitudinally polarized W^- must be attributed to the component in which both W 's are longitudinal.

We have also examined a \mathcal{Z}_2 -symmetric Singlet extension of the SM with an additional heavy scalar [49–63]. In this model the couplings of the two Higgses to SM particles are proportional to the SM couplings of the Higgs, multiplied by universal factors:

$$g_{xxs} = g_{xxh}^{\text{SM}}(1 + \Delta_{xs}) \quad \text{with} \quad 1 + \Delta_{xs} = \begin{cases} \cos \alpha & s = h \\ \sin \alpha & s = H \end{cases}, \quad (8.1)$$

$$g_{xxs_1s_2} = g_{xxhh}^{\text{SM}}(1 + \Delta_{xs_1})(1 + \Delta_{xs_2}), \quad (8.2)$$

where xx represents a pair of SM fermions or vectors, and α is the mixing angle. As a consequence, since only small values of $\sin \alpha$ are allowed [64–66], the width of the heavy Higgs is much smaller than the width of a SM Higgs of the same mass. We have taken $\sin \alpha = 0.2$, $m_H = 600$ GeV and $\tan \beta = 0.3$, where $\tan \beta$ is the ratio of the vacuum expectation values of the two neutral scalar fields, which yields $\Gamma_H = 6.45$ GeV.

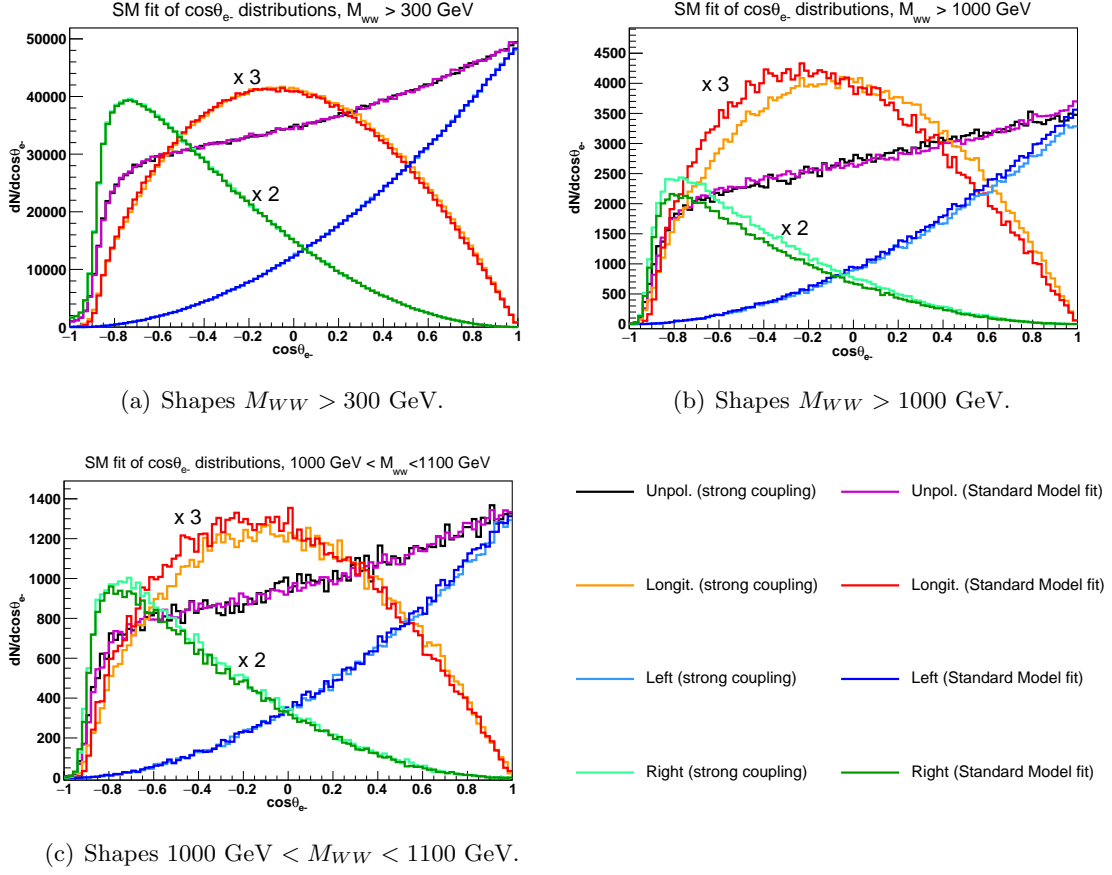


Figure 9. Shape comparison between SM and Higgsless generation. $p_t^e > 20$ GeV, $|\eta^e| < 2.5$. The longitudinal and right handed components have been multiplied by three and two, respectively.

With the exception of the mass window in the vicinity of the heavy Higgs resonance all results for the Singlet model follow closely those of the SM.

We have checked that, for each W polarization, the shape of charged lepton angular distributions, $1/\sigma \cdot d\sigma/d\cos\theta$, in both the singlet and the noHiggs models, are in reasonable agreement with the corresponding SM shape in all 100 GeV intervals in the WW invariant mass, even though the normalizations can be quite different. We have also verified the agreement between the sum of singly polarized distributions and the full result in both cases.

The results are shown in fig. 9 for the Higgsless model, and in fig. 10 for the Singlet one. In both figures the black histogram shows the result of the full calculation. The lighter red, green and blue curves are the singly polarized distributions in the Higgsless and Singlet models. The darker red, green and blue curves show the results for the longitudinal, right and left handed polarizations, respectively, of the fit of the full results using the SM templates. The longitudinal and right handed components have been multiplied by three and two, respectively, to improve the overall readability of the plots.

Fig. 9(a) and fig. 10(a) show that, when a large range of invariant masses is taken

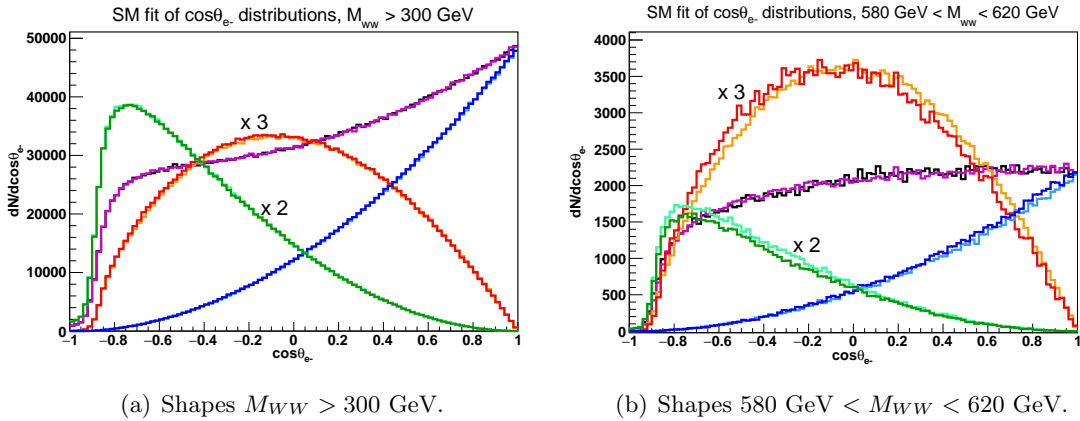


Figure 10. Shape comparison between SM and Singlet generation. Lines as in fig. 9. $p_t^e > 20$ GeV, $|\eta^e| < 2.5$. The longitudinal and right handed components have been multiplied by three and two, respectively.

into account, the shapes of the polarized components are indeed very similar in the three models. This is not surprising since the distributions are dominated by low invariant mass events, for which the differences between the various models are expected to be small.

Fig. 9(b), fig. 9(c) and fig. 10(b) show that, when restricting the comparison to large invariant masses, the shapes of the left and right handed components remain quite similar in the various models, while the shape of the longitudinal component in the Higgsless and Singlet model appears slightly shifted to large values of $\cos\theta$ in comparison with the SM distribution. The effect seems to increase for increasing M_{WW} , in fact, it is more pronounced in fig. 9(b), which contains events of higher average mass, than in fig. 9(c).

Despite these differences, the fit of both models using SM templates is quite good. We have fitted the full result for each model, by means of a χ^2 minimization, with a linear combination of four normalized functions extracted from the SM distributions: the shapes for the longitudinal, right and left handed components together with the shape of the SM interference. The latter is defined as the normalized difference between the unpolarized, full distribution and the sum of the three singly polarized ones.

In tab. 1, we show a selection of results. The rows labeled SM, no Higgs and Singlet show the percent ratio of the singly polarized cross sections to the full, unpolarized cross section for each model. The rows labeled Fit give the coefficients, in percent, of the four SM shapes obtained from the fit of the angular distribution of the electron in the corresponding model.

When the fit is extended to the full range of invariant masses, $M_{WW} > 300$ GeV, the polarization fractions returned by the fit reproduce the results obtained from the ratio of the OSP polarized cross sections to the full one.

For the Higgsless model, we have investigated the agreement between these two determinations of the polarization fractions in each 100 GeV interval in the WW invariant mass. The accord is quite good in each bin, even though the normalizations become progressively different as the invariant mass grows.

	Long.	L	R	Int.
$M_{WW} > 300$ GeV				
SM	21	52	25	2
no Higgs	27	48	23	2
Fit no Higgs	26	48	23	2
Singlet	23	51	24	2
Fit Singlet	23	51	24	2
$M_{WW} > 1000$ GeV				
SM	15	58	22	4
no Higgs	35	45	17	3
Fit no Higgs	35	47	15	2
580 GeV $< M_{WW} < 620$ GeV				
SM	19	53	25	3
Singlet	42	38	18	2
Fit Singlet	42	40	17	2

Table 1. The rows labeled SM, no Higgs and Singlet show the percent ratio of the polarized cross sections to the full result. The rows labeled Fit give the coefficients, in percent, extracted from a χ^2 fit of a linear combination of the SM shapes for the longitudinal, left, right handed components and the interference to the full unpolarized angular distribution in the corresponding model.

The $M_{WW} > 1000$ GeV range, where the longitudinal polarization fractions in the Higgsless model is more than twice the SM one, gives the poorest agreement. However, the discrepancy between the polarization fractions from the fit and those from the ratio of cross sections is of the order of 10% at most.

The fitted polarization fractions for the Singlet model in the heavy Higgs peak region, 580 GeV $< M_{WW} < 620$ GeV, are in very good agreement with those estimated from the ratio of the singly polarized cross sections to the full result in that bin.

The results presented in this section suggest that it is possible to extract the polarization fractions of the W in an almost model-independent way, exploiting the similarity of the shapes of polarized $\cos\theta_e$ distributions for different underlying theories, in most kinematic regions.

The angular distributions we have discussed, are difficult to measure, particularly when both W 's decay leptonically. However, the same approach can be applied to other kinematic variables whose distributions discriminate among the different polarizations, as for instance the invariant mass of the charged lepton pair and the transverse momentum of the charged lepton, as shown in fig. 6. In order to enhance the accuracy of the obtained results, more refined multivariate fit methods could be investigated.

9 Conclusions

In this paper we have investigated the possibility of defining cross sections for processes with polarized W bosons, including off shell and non resonant effects.

We have proposed a method which is based on the observation that the set of doubly resonant diagrams, suitably projected on shell to preserve gauge invariance, approximates well the full result and allows an expansion in terms of amplitudes in which each final state W has a definite polarization. This procedure agrees with the standard approach based on Legendre polynomials in the absence of cuts on the decay leptons. When acceptance cuts are imposed on the leptons, and the Legendre polynomials procedure fails, it is possible to extract the polarization fractions using singly polarized SM Monte Carlo templates. These same templates can be used to measure the polarization of the W with reasonable accuracy even if new physics is present.

Acknowledgements

Discussions with Pietro Govoni have been invaluable and are gratefully acknowledged. The authors would like to acknowledge the contribution of the COST Action CA16108.

Appendix A Numerical effects of different approximations in the large mass, large transverse momentum region.

In this appendix we exemplify how different, gauge invariance violating approximations in the calculation of amplitudes may produce unreliable results in the large energy regime.

We study two instances. The first one is the naive way to isolate the resonant contribution to W^+W^- production in VBF, by simply dropping all other diagrams and requiring the invariant mass of each $\ell\nu$ pair to be close to the W mass. In the second one, we examine quantitatively the relevance of non null vector boson widths in the OSP projected amplitudes. All the results in this Appendix refer to the Standard Model.

A.1 Resonant contributions and gauge cancellations

The first approximation is based on the intuitive notion that the closer the invariant mass of the lepton–neutrino system to the mass of the W boson, the more dominant the resonant diagrams are ¹. Therefore, it is reasonable to expect that by restricting the invariant mass of each $\ell\nu$ pair around M_W , the non resonant diagrams can be neglected.

In order to have a reference point for the size of possible effects, we have computed separately, without any constraint on the invariant masses of the lepton–neutrino pairs, the contribution of the doubly resonant diagrams and of the complementary set of diagrams, that is, those which are singly resonant or non resonant, which we will refer to as non resonant for simplicity.

¹This contribution can be computed in MadGraph5 generating the process:

$p p > j j w^+ w^-, w^+ > \mu^+ \nu_\mu, w^- > e^- \nu_e.$

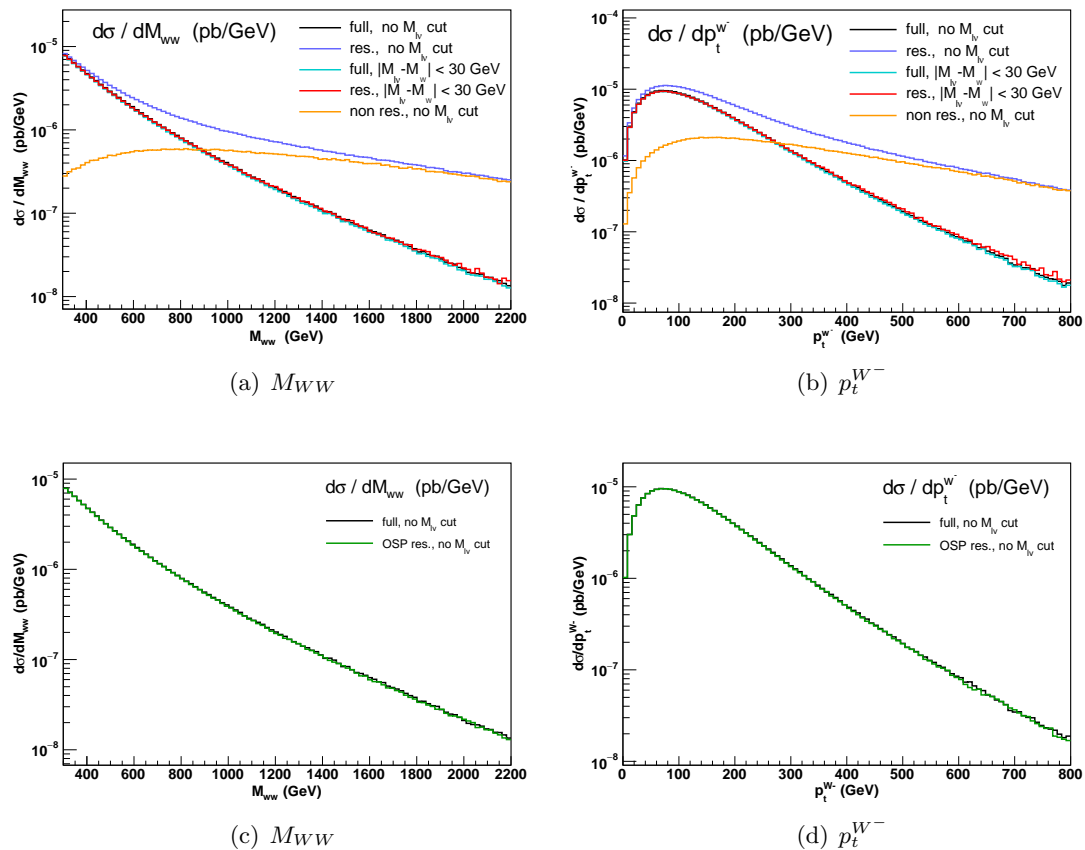


Figure 11. Differential cross sections as a function of M_{WW} and $p_t^{W^-}$ under different assumptions. In black the full results without cuts on the lepton system; in light blue the full result with the constraint $|M_{\ell\nu} - M_W| < 30$ GeV for each $\ell\nu$ pair. The blue–violet, red and green histograms are computed using only the resonant diagrams. The blue–violet curves are obtained without lepton cuts; the red ones requiring $|M_{\ell\nu} - M_W| < 30$ GeV; the green plots are the result of the OSP without any restriction on the lepton–neutrino system.

Then, we have restricted the mass of electron neutrino pair to a neighborhood of the W mass. Specifically, we have required $|M_{\ell\nu} - M_W| < 30$ GeV as a compromise between minimizing the non resonant contribution and constraining too much a variable which cannot be measured precisely at hadron–hadron colliders. We have also tried narrower intervals, finding similar results.

In the upper row of fig. 11 we present the differential distribution of the four lepton mass (left) and of the transverse momentum of the $\ell^- \nu$ pair (right). The result obtained from the full calculation, without any restriction on the lepton–neutrino system is shown in black. We compare it with the full results obtained restricting the mass of each $\ell\nu$ pair to $|M_{\ell\nu} - M_W| < 30$ GeV (light blue). Clearly, the two distributions agree quite well over the full range in M_{WW} and $p_t^{W^-}$, showing that, as expected, in most of the events, the mass of the $\ell\nu$ system is close to M_W . In the same plots we also show the results, obtained

Region	Full	Resonant	Non-resonant	Interference
$50 \text{ GeV} < M_{e^{-}\nu} < 110 \text{ GeV},$ $50 \text{ GeV} < M_{\mu^{+}\nu} < 110 \text{ GeV}$	$3.975 \cdot 10^{-5}$	$4.233 \cdot 10^{-5}$	$2.670 \cdot 10^{-6}$	$-5.244 \cdot 10^{-6}$
$50 \text{ GeV} < M_{e^{-}\nu} < 110 \text{ GeV},$ $M_{\mu^{+}\nu} > 110 \text{ GeV}$	$1.050 \cdot 10^{-6}$	$1.574 \cdot 10^{-4}$	$1.554 \cdot 10^{-4}$	$-3.118 \cdot 10^{-4}$
$M_{e^{-}\nu} > 110 \text{ GeV},$ $50 \text{ GeV} < M_{\mu^{+}\nu} < 110 \text{ GeV}$	$1.065 \cdot 10^{-6}$	$1.587 \cdot 10^{-4}$	$1.584 \cdot 10^{-4}$	$-3.161 \cdot 10^{-4}$
$M_{e^{-}\nu} > 110 \text{ GeV},$ $M_{\mu^{+}\nu} > 110 \text{ GeV}$	$3.751 \cdot 10^{-8}$	$1.693 \cdot 10^{-4}$	$1.693 \cdot 10^{-4}$	$-3.386 \cdot 10^{-4}$

Table 2. Cross-sections (pb) in different $M_{e^{-}\nu}, M_{\mu^{+}\nu}$ regions, for $M_{ww} > 1400 \text{ GeV}$.

over the full leptonic phase space, taking into account only the doubly resonant diagrams (blue-violet) and those obtained taking into account only the non resonant ones (yellow). Finally, the distribution obtained from the doubly resonant diagrams with the additional constraint $|M_{\ell\nu} - M_W| < 30 \text{ GeV}$ is given in red.

For completeness, in the lower part of fig. 11 we show that the distributions from the full calculation agree very well, for both variables, with those produced by the coherent sum of OSP projections.

The comparison between the black histogram, the blue-violet and the yellow curves demonstrates that the resonant and non resonant diagrams interfere strongly and that, in the absence of cuts on $M_{\ell\nu}$, the set of resonant diagrams does not reproduce well the correct result, the discrepancy increasing with increasing invariant mass or transverse momentum of the lepton-neutrino pair.

However, as shown by the red histogram, if the mass of the individual $\ell\nu$ pair is forced to be sufficiently close to the W mass, the set of resonant diagrams describes rather well the full results, at least on a logarithmic scale.

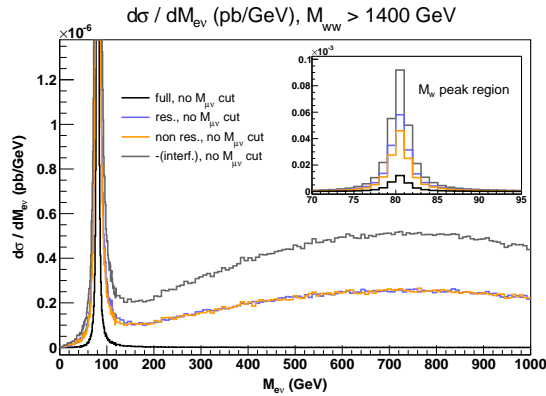


Figure 12. Invariant mass distribution of the $e^{-}\bar{\nu}_e$ pair for $M_{WW} > 1400 \text{ GeV}$ in the SM results. No cuts on leptons.

Nevertheless, if the comparison between the full calculation and the naive approximation is pushed to the high invariant mass, high p_t , region, the latter fails to reproduce the full result.

In fig. 12 we show the distribution of the invariant mass of the $M_{e-\nu}$ pair for $M_{WW} > 1400$ GeV. No additional cut is imposed on any lepton. The region close to M_W is highlighted in the insert. The color code is as in fig. 11: the black curve refers to the full result; the blue-violet histogram is computed using only the resonant diagrams; the yellow curve is obtained from the non resonant set of diagrams. The gray curve shows the interference contribution, with opposite sign with respect to its actual value, and refers to the difference between the full result and the sum of the resonant and non resonant one.

Two features leap to the eye: the large interference between the resonant and non resonant diagrams, even in the vicinity of the M_W peak and the enhancement at large invariant masses which, while about two orders of magnitude smaller than the peak, extends over a very large region.

Additional information is provided in tab. 2 which shows the total cross section in different zones in the $M_{e-\nu}$, $M_{\mu+\nu}$ plane, separating the region close to the mass of the W from the large mass one.

Tab. 2 shows a discrepancy of about 5% between the full result and the doubly resonant cross section already when both lepton neutrino pairs are close to the W mass shell. This shows, as anticipated, that, in this regime, restricting the mass of both pairs to within 30 GeV from the W mass is not enough to reproduce the full results using only the resonant contribution.

Furthermore, for both the resonant diagrams and the non resonant ones, the cross section in the regions in which one of the pairs is in the vicinity of the W peak while the other is outside this region and in the region in which both pairs are off shell are large, about four times larger than the full cross section when both lepton-neutrino pairs are nearly on shell. However, in each of these three regions, the contribution of the resonant diagrams and the contribution from non resonant ones cancel each other to better than 1 percent when only one of the pairs has a mass close to M_W , and to about 2 per mill when both are off shell, leading to the expected physical distribution dominated by the Breit-Wigner peak.

The enhancement at large invariant masses in the $M_{e-\nu}$ distribution in fig. 12 can be qualitatively understood as follows. Let's consider the subset of the doubly resonant diagrams in which vector bosons scatter among themselves as in fig. 1(a). These are in one to one correspondence with the set of diagrams which describe the scattering among on shell vector bosons. Furthermore let's keep fixed the initial and final quark momenta, so that the space-like invariant mass of each of the two virtual W 's entering the scattering and the total mass of the two bosons which decay to the final state leptons are also fixed.

In the scattering between longitudinally polarized vector bosons, the leading term of each diagram without Higgs exchange grows as s^2 . The sum of all these diagrams however grows only like s , because the sum of the leading terms turns out to be proportional to $s + t + u$, which corresponds to the sum of the masses squared of the bosons participating in the scattering, decreasing by one unit the degree of divergence.

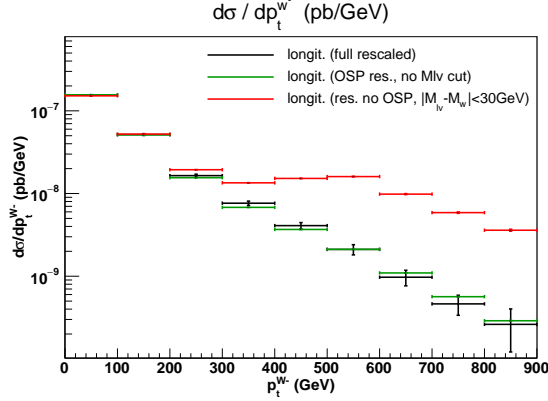


Figure 13. Transverse momentum distribution of longitudinally polarized W^- for $M_{WW} > 1000$ GeV. The full result is shown in black; the OSP one, in green. The red points are obtained neglecting non resonant diagrams and requiring $|M_{\ell\nu} - M_W| < 30$ GeV. The red and green results have been obtained with a fixed polarization for the negatively charged W . The black points have been computed from a generation of the full process, extracting the longitudinal fraction f_0 in each transverse momentum bin through a Legendre expansion, cfr sect. 2.

The dominant behaviour for the corresponding diagrams with off shell vector bosons can be extracted substituting

$$-g^{\mu\nu} + \frac{k^\mu k^\nu}{M^2} \rightarrow \varepsilon_0^\mu \varepsilon_0^{\nu*} \quad (\text{A.1})$$

in each propagator, that is, taking into account the contribution with all intermediate vector bosons longitudinally polarized.

At high energy, $\varepsilon_0^\mu(k) = k^\mu/M + \mathcal{O}(1)$. When the polarization vectors act on the external fermion lines, the term proportional to the momentum gives zero and no enhancement is produced. The remaining part of each diagram in the set under consideration, has the same analytic expression of the corresponding on shell diagram, with the difference that the boson momenta are not on their mass shell.

The sum of the leading contributions again reduces to $s + t + u$, but in this case the external “masses” do not coincide with their on shell values, and can become large when the time-like vector bosons are highly off shell, compensating the effect of the large denominators in the vector propagators. Eventually this enhancement will be cut off by phase space constraints for very large values of $M_{e-\nu}$.

As a further proof that all issues related to anomalous behaviours at high energy are connected with the longitudinal polarization of the vector bosons, we present, in fig. 13, the transverse momentum distribution of the longitudinally polarized W^- for events with $M_{WW} > 1000$ GeV. The full result is shown in black; the OSP one, in green. The red points are obtained neglecting non resonant diagrams and requiring $|M_{\ell\nu} - M_W| < 30$ GeV. In all cases the W^+ is unpolarized and no cut on the leptonic variables is applied. While the OSP prediction agrees with the full result over the whole range, the curve obtained requiring $|M_{\ell\nu} - M_W| < 30$ GeV overshoots the true result by a large factor for transverse

momenta above 300 GeV, confirming that this naive approximation cannot be relied on in the high energy regime.

A.2 Vector boson widths in the OSP method

We now move to the second example, namely computing the OSP amplitudes in the CMSc scheme, instead of setting the weak bosons widths to zero and using real couplings. Typically, for an amplitude without internal vector bosons which can go on mass shell, the difference between the CMSc and setting all widths to zero is small, of order $\mathcal{O}(\Gamma/M) = \mathcal{O}(\alpha)$. However, when the energy of the vector bosons grows large, these differences can become significant, because any deviation from a fully gauge invariant treatment of the boson widths spoils the cancellation of terms which are proportional to the energy.

In order to examine quantitatively the relevance of these gauge violating effects in VBS, we study the single process $uu \rightarrow uu e^- \bar{\nu}_e \mu^+ \nu_\mu$, for large invariant masses of the four lepton system, $M_{WW} > 1000$ GeV, large transverse momentum of the $e^- \bar{\nu}_e$ pair, $p_t^{W^-} > 800$ GeV. The mass of each pair is required to be very close to the W mass, $|M_{\ell\nu} - M_W| < 0.2$ GeV. No further cut on the charged leptons are applied.

A full calculation in the Complex Mass Scheme gives a cross section of $0.641(3) \cdot 10^{-8}$ pb, which we regard as the true result. We then recompute the cross section restricting the calculation to the doubly resonant diagrams and projecting them on mass shell, as discussed in sect. 3, employing two different prescriptions for masses and couplings. Using complex masses and couplings, as in the CMSc, yields $0.754(2) \cdot 10^{-8}$ pb, which is not compatible with the correct value. However, when all masses and couplings are taken to be real, as advocated in sect. 3, the result is $0.650(2) \cdot 10^{-8}$ pb, in excellent agreement with the cross section obtained from the full calculation. This proves again, in our opinion, that failing to maintain gauge invariance could indeed lead to significantly flawed results. Obviously, it does not prove that any gauge invariant calculation would reproduce the correct answer. In particular, the correctness and usefulness of the projection procedure needs to be verified in each case.

Gauge effects are particularly strong for longitudinally polarized vector bosons. Therefore, we have also computed the on shell projected cross sections for a longitudinally polarized W^- : using complex masses and couplings we obtain $1.282(5) \cdot 10^{-9}$ pb, while, taking them to be real gives $0.202(1) \cdot 10^{-9}$ pb, which differ by a factor of about six. Notice that the difference between these two cross sections is equal, within errors, to the difference between the corresponding unpolarized results, suggesting that the discrepancy between the results for longitudinally polarized W^- accounts for the totality of the difference in the unpolarized case.

Since no cuts on the charged lepton is imposed, the cross section for a longitudinally polarized W boson can also be extracted from the full distribution, projecting on Legendre polynomials. This yields $0.211(5) \cdot 10^{-9}$ pb, confirming the OSP result with all internal widths set to zero.

References

- [1] **ATLAS** Collaboration, G. Aad et al., *Observation of a new particle in the search for the Standard Model Higgs boson with the ATLAS detector at the LHC*, *Phys.Lett.* **B716** (2012) 1–29, [[arXiv:1207.7214](#)].
- [2] **CMS** Collaboration, S. Chatrchyan et al., *Observation of a new boson at a mass of 125 GeV with the CMS experiment at the LHC*, *Phys.Lett.* **B716** (2012) 30–61, [[arXiv:1207.7235](#)].
- [3] **ATLAS, CMS** Collaboration, G. Aad et al., *Combined Measurement of the Higgs Boson Mass in pp Collisions at $\sqrt{s} = 7$ and 8 TeV with the ATLAS and CMS Experiments*, *Phys.Rev.Lett.* **114** (2015) 191803, [[arXiv:1503.07589](#)].
- [4] **ATLAS, CMS** Collaboration, G. Aad et al., *Measurements of the Higgs boson production and decay rates and constraints on its couplings from a combined ATLAS and CMS analysis of the LHC pp collision data at $\sqrt{s} = 7$ and 8 TeV*, *JHEP* **08** (2016) 045, [[arXiv:1606.02266](#)].
- [5] M. J. Duncan, G. L. Kane, and W. W. Repko, *W W Physics at Future Colliders*, *Nucl. Phys.* **B272** (1986) 517–559.
- [6] D. A. Dicus and R. Vega, *WW Production From PP Collisions*, *Phys. Rev. Lett.* **57** (1986) 1110–1112.
- [7] R. Kleiss and W. J. Stirling, *Tagging the Higgs*, *Phys. Lett.* **B200** (1988) 193–199.
- [8] V. D. Barger, K.-m. Cheung, T. Han, and R. J. N. Phillips, *Strong W^+W^+ scattering signals at pp supercolliders*, *Phys. Rev.* **D42** (1990) 3052–3077.
- [9] U. Baur and E. W. N. Glover, *Tagging the Higgs boson in $pp \rightarrow W^+W^-jj$* , *Phys. Lett.* **B252** (1990) 683–689.
- [10] D. A. Dicus, J. F. Gunion, and R. Vega, *Isolating the scattering of longitudinal W^+ ’s at the SSC using like sign dileptons*, *Phys. Lett.* **B258** (1991) 475–481.
- [11] D. A. Dicus, J. F. Gunion, L. H. Orr, and R. Vega, *Isolating purely leptonic signals for strong W scattering using antitagging jet tagging, and lepton isolation*, *Nucl. Phys.* **B377** (1992) 31–54.
- [12] J. Bagger, V. D. Barger, K.-m. Cheung, J. F. Gunion, T. Han, G. A. Ladinsky, R. Rosenfeld, and C. P. Yuan, *CERN LHC analysis of the strongly interacting $W W$ system: Gold plated modes*, *Phys. Rev.* **D52** (1995) 3878–3889, [[hep-ph/9504426](#)].
- [13] K. Iordanidis and D. Zeppenfeld, *Searching for a heavy Higgs boson via the $H \rightarrow$ lepton neutrino jet jet mode at the CERN LHC*, *Phys. Rev.* **D57** (1998) 3072–3083, [[hep-ph/9709506](#)].
- [14] J. M. Butterworth, B. E. Cox, and J. R. Forshaw, *WW scattering at the CERN LHC*, *Phys. Rev.* **D65** (2002) 096014, [[hep-ph/0201098](#)].
- [15] E. Accomando, A. Ballestrero, S. Bolognesi, E. Maina, and C. Mariotti, *Boson-boson scattering and Higgs production at the LHC from a six fermion point of view: Four jets + $\ell\nu$ processes at $O(\alpha_{em}^6)$* , *JHEP* **03** (2006) 093, [[hep-ph/0512219](#)].
- [16] A. Alboteanu, W. Kilian, and J. Reuter, *Resonances and Unitarity in Weak Boson Scattering at the LHC*, *JHEP* **11** (2008) 010, [[arXiv:0806.4145](#)].

- [17] C. Englert, B. Jager, M. Worek, and D. Zeppenfeld, *Observing Strongly Interacting Vector Boson Systems at the CERN Large Hadron Collider*, *Phys. Rev.* **D80** (2009) 035027, [[arXiv:0810.4861](#)].
- [18] A. Ballestrero, G. Bevilacqua, and E. Maina, *A Complete parton level analysis of boson-boson scattering and ElectroWeak Symmetry Breaking in $l\nu + \text{four jets}$ production at the LHC*, *JHEP* **05** (2009) 015, [[arXiv:0812.5084](#)].
- [19] A. Ballestrero, G. Bevilacqua, D. Buarque Franzosi, and E. Maina, *How well can the LHC distinguish between the SM light Higgs scenario, a composite Higgs and the Higgsless case using VV scattering channels?*, *JHEP* **11** (2009) 126, [[arXiv:0909.3838](#)].
- [20] A. Ballestrero, D. Buarque Franzosi, and E. Maina, *Vector-Vector scattering at the LHC with two charged leptons and two neutrinos in the final state*, *JHEP* **06** (2011) 013, [[arXiv:1011.1514](#)].
- [21] **LHC Higgs Cross Section Working Group** Collaboration, S. Dittmaier et al., *Handbook of LHC Higgs Cross Sections: 1. Inclusive Observables*, [arXiv:1101.0593](#).
- [22] S. Dittmaier et al., *Handbook of LHC Higgs Cross Sections: 2. Differential Distributions*, [arXiv:1201.3084](#).
- [23] **LHC Higgs Cross Section Working Group** Collaboration, J. R. Andersen et al., *Handbook of LHC Higgs Cross Sections: 3. Higgs Properties*, [arXiv:1307.1347](#).
- [24] **LHC Higgs Cross Section Working Group** Collaboration, D. de Florian et al., *Handbook of LHC Higgs Cross Sections: 4. Deciphering the Nature of the Higgs Sector*, [arXiv:1610.07922](#).
- [25] Z. Bern et al., *Left-Handed W Bosons at the LHC*, *Phys. Rev.* **D84** (2011) 034008, [[arXiv:1103.5445](#)].
- [26] W. J. Stirling and E. Vryonidou, *Electroweak gauge boson polarisation at the LHC*, *JHEP* **07** (2012) 124, [[arXiv:1204.6427](#)].
- [27] A. Belyaev and D. Ross, *What Does the CMS Measurement of W-polarization Tell Us about the Underlying Theory of the Coupling of W-Bosons to Matter?*, *JHEP* **08** (2013) 120, [[arXiv:1303.3297](#)].
- [28] **CMS** Collaboration, S. Chatrchyan et al., *Measurement of the Polarization of W Bosons with Large Transverse Momenta in $W+\text{Jets}$ Events at the LHC*, *Phys. Rev. Lett.* **107** (2011) 021802, [[arXiv:1104.3829](#)].
- [29] **ATLAS** Collaboration, G. Aad et al., *Measurement of the polarisation of W bosons produced with large transverse momentum in pp collisions at $\sqrt{s} = 7$ TeV with the ATLAS experiment*, *Eur. Phys. J.* **C72** (2012) 2001, [[arXiv:1203.2165](#)].
- [30] **ATLAS** Collaboration, M. Aaboud et al., *Measurement of the W boson polarisation in $t\bar{t}$ events from pp collisions at $\sqrt{s} = 8$ TeV in the lepton+jets channel with ATLAS*, [arXiv:1612.02577](#).
- [31] **CMS** Collaboration, V. Khachatryan et al., *Measurement of the W boson helicity fractions in the decays of top quark pairs to lepton + jets final states produced in pp collisions at $\sqrt{s} = 8$ TeV*, *Phys. Lett.* **B762** (2016) 512–534, [[arXiv:1605.09047](#)].
- [32] K. Doroba, J. Kalinowski, J. Kuczmarski, S. Pokorski, J. Rosiek, M. Szeleper, and S. Tkaczyk, *The $W_L W_L$ Scattering at the LHC: Improving the Selection Criteria*, *Phys. Rev.* **D86** (2012) 036011, [[arXiv:1201.2768](#)].

- [33] B. Jager, C. Oleari, and D. Zeppenfeld, *Next-to-leading order QCD corrections to W^+W^- production via vector-boson fusion*, *JHEP* **07** (2006) 015, [[hep-ph/0603177](#)].
- [34] B. Jager and G. Zanderighi, *Electroweak W^+W^-jj production at NLO in QCD matched with parton shower in the POWHEG-BOX*, *JHEP* **04** (2013) 024, [[arXiv:1301.1695](#)].
- [35] B. Biedermann, A. Denner, and M. Pellen, *Large electroweak corrections to vector-boson scattering at the Large Hadron Collider*, [arXiv:1611.02951](#).
- [36] A. Kadeer, J. G. Korner, and U. Moosbrugger, *Helicity analysis of semileptonic hyperon decays including lepton mass effects*, *Eur. Phys. J.* **C59** (2009) 27–47, [[hep-ph/0511019](#)].
- [37] A. Ballestrero, A. Belhouari, G. Bevilacqua, V. Kashkan, and E. Maina, *PHANTOM: A Monte Carlo event generator for six parton final states at high energy colliders*, *Comput.Phys.Commun.* **180** (2009) 401–417, [[arXiv:0801.3359](#)].
- [38] A. Aeppli, F. Cuypers, and G. J. van Oldenborgh, *$O(\Gamma)$ corrections to W pair production in e^+e^- and $\gamma\gamma$ collisions*, *Phys. Lett.* **B314** (1993) 413–420, [[hep-ph/9303236](#)].
- [39] A. Aeppli, G. J. van Oldenborgh, and D. Wyler, *Unstable particles in one loop calculations*, *Nucl. Phys.* **B428** (1994) 126–146, [[hep-ph/9312212](#)].
- [40] A. Denner, S. Dittmaier, M. Roth, and D. Wackerroth, *Electroweak radiative corrections to $e^+e^- \rightarrow WW \rightarrow 4$ fermions in double pole approximation: The RACOONWW approach*, *Nucl. Phys.* **B587** (2000) 67–117, [[hep-ph/0006307](#)].
- [41] M. Billoni, S. Dittmaier, B. Jager, and C. Speckner, *Next-to-leading order electroweak corrections to $pp \rightarrow W^+W^- \rightarrow 4$ leptons at the LHC in double-pole approximation*, *JHEP* **12** (2013) 043, [[arXiv:1310.1564](#)].
- [42] B. Biedermann, M. Billoni, A. Denner, S. Dittmaier, L. Hofer, B. Jager, and L. Salfelder, *Next-to-leading-order electroweak corrections to $pp \rightarrow W^+W^- \rightarrow 4$ leptons at the LHC*, *JHEP* **06** (2016) 065, [[arXiv:1605.03419](#)].
- [43] J. Alwall et al., *A standard format for Les Houches event files*, *Comput. Phys. Commun.* **176** (2007) 300–304, [[hep-ph/0609017](#)].
- [44] E. N. Argyres, W. Beenakker, G. J. van Oldenborgh, A. Denner, S. Dittmaier, J. Hoogland, R. Kleiss, C. G. Papadopoulos, and G. Passarino, *Stable calculations for unstable particles: Restoring gauge invariance*, *Phys. Lett.* **B358** (1995) 339–346, [[hep-ph/9507216](#)].
- [45] W. Beenakker, G. J. van Oldenborgh, A. Denner, S. Dittmaier, J. Hoogland, R. Kleiss, C. G. Papadopoulos, and G. Passarino, *The Fermion loop scheme for finite width effects in e^+e^- annihilation into four fermions*, *Nucl. Phys.* **B500** (1997) 255–298, [[hep-ph/9612260](#)].
- [46] E. Accomando, A. Ballestrero, and E. Maina, *Nonconserved currents and gauge restoring schemes in single W production*, *Phys. Lett.* **B479** (2000) 209–217, [[hep-ph/9911489](#)].
- [47] A. Denner, S. Dittmaier, M. Roth, and L. H. Wieders, *Electroweak corrections to charged-current $e^+e^- \rightarrow 4$ fermion processes: Technical details and further results*, *Nucl. Phys.* **B724** (2005) 247–294, [[hep-ph/0505042](#)]. [Erratum: *Nucl. Phys.*B854,504(2012)].
- [48] NNPDF Collaboration, R. D. Ball et al., *Parton distributions for the LHC Run II*, *JHEP* **04** (2015) 040, [[arXiv:1410.8849](#)].
- [49] V. Silveira and A. Zee, *Scalar Phantoms*, *Phys.Lett.* **B161** (1985) 136.
- [50] R. Schabinger and J. D. Wells, *A Minimal spontaneously broken hidden sector and its impact*

- on Higgs boson physics at the large hadron collider, *Phys.Rev.* **D72** (2005) 093007, [[hep-ph/0509209](#)].
- [51] D. O’Connell, M. J. Ramsey-Musolf, and M. B. Wise, *Minimal Extension of the Standard Model Scalar Sector*, *Phys.Rev.* **D75** (2007) 037701, [[hep-ph/0611014](#)].
- [52] O. Bahat-Treidel, Y. Grossman, and Y. Rozen, *Hiding the Higgs at the LHC*, *JHEP* **0705** (2007) 022, [[hep-ph/0611162](#)].
- [53] V. Barger, P. Langacker, M. McCaskey, M. J. Ramsey-Musolf, and G. Shaughnessy, *LHC Phenomenology of an Extended Standard Model with a Real Scalar Singlet*, *Phys.Rev.* **D77** (2008) 035005, [[arXiv:0706.4311](#)].
- [54] G. Bhattacharyya, G. C. Branco, and S. Nandi, *Universal Doublet-Singlet Higgs Couplings and phenomenology at the CERN Large Hadron Collider*, *Phys.Rev.* **D77** (2008) 117701, [[arXiv:0712.2693](#)].
- [55] M. Gonderinger, Y. Li, H. Patel, and M. J. Ramsey-Musolf, *Vacuum Stability, Perturbativity, and Scalar Singlet Dark Matter*, *JHEP* **1001** (2010) 053, [[arXiv:0910.3167](#)].
- [56] S. Dawson and W. Yan, *Hiding the Higgs Boson with Multiple Scalars*, *Phys.Rev.* **D79** (2009) 095002, [[arXiv:0904.2005](#)].
- [57] S. Bock, R. Lafaye, T. Plehn, M. Rauch, D. Zerwas, et al., *Measuring Hidden Higgs and Strongly-Interacting Higgs Scenarios*, *Phys.Lett.* **B694** (2010) 44–53, [[arXiv:1007.2645](#)].
- [58] P. J. Fox, D. Tucker-Smith, and N. Weiner, *Higgs friends and counterfeits at hadron colliders*, *JHEP* **1106** (2011) 127, [[arXiv:1104.5450](#)].
- [59] C. Englert, T. Plehn, D. Zerwas, and P. M. Zerwas, *Exploring the Higgs portal*, *Phys.Lett.* **B703** (2011) 298–305, [[arXiv:1106.3097](#)].
- [60] C. Englert, J. Jaeckel, E. Re, and M. Spannowsky, *Evasive Higgs Maneuvers at the LHC*, *Phys.Rev.* **D85** (2012) 035008, [[arXiv:1111.1719](#)].
- [61] B. Batell, S. Gori, and L.-T. Wang, *Exploring the Higgs Portal with 10/fb at the LHC*, *JHEP* **1206** (2012) 172, [[arXiv:1112.5180](#)].
- [62] C. Englert, T. Plehn, M. Rauch, D. Zerwas, and P. M. Zerwas, *LHC: Standard Higgs and Hidden Higgs*, *Phys.Lett.* **B707** (2012) 512–516, [[arXiv:1112.3007](#)].
- [63] R. S. Gupta and J. D. Wells, *Higgs boson search significance deformations due to mixed-in scalars*, *Phys.Lett.* **B710** (2012) 154–158, [[arXiv:1110.0824](#)].
- [64] G. M. Pruna and T. Robens, *The Higgs Singlet extension parameter space in the light of the LHC discovery*, *Phys.Rev.* **D88** (2013) 115012, [[arXiv:1303.1150](#)].
- [65] D. López-Val and T. Robens, *r and the W -boson mass in the singlet extension of the standard model*, *Phys.Rev.* **D90** (2014), no. 11 114018, [[arXiv:1406.1043](#)].
- [66] T. Robens and T. Stefaniak, *Status of the Higgs Singlet Extension of the Standard Model after LHC Run 1*, *Eur.Phys.J.* **C75** (2015), no. 3 104, [[arXiv:1501.02234](#)].